materials

MDPI

Article

Effects of Ni and Cu Residuals on the Magnetic Properties and Microstructure of $SmCo_5$ Magnets

Muhammad Farhan Mehmood [1,2,*], Anas Eldosouky [3], Kristina Žužek Rožman [1,2] and Sašo Šturm [1,2]

[1] Jožef Stefan International Postgraduate School, Jamova 39, SI-1000 Ljubljana, Slovenia
[2] Department for Nanostructured Materials, Jožef Stefan Institute, Jamova 39, SI-1000 Ljubljana, Slovenia
[3] Magneti Ljubljana, d.d. Stegne 37, SI-1000 Ljubljana, Slovenia
* Correspondence: mehmood.mfarhan@gmail.com

Abstract: The effect of Ni/Cu-coating residuals on the magnetic properties and microstructures of samarium–cobalt ($SmCo_5$) magnets was studied. $SmCo_5$ magnets with 0.0, 0.5, 1.0, 2.0, 3.0 and 4.0 wt.% of added Ni/Cu (85 wt.% Ni/15 wt.% Cu) were prepared using a conventional sintering route. The magnetic properties of the magnets were found to be consistent up to 2 wt.% Ni/Cu. Any further increase in the Ni/Cu content resulted in a significant reduction in the magnetic properties, to lower than values that would be commercially acceptable. SEM/EDS studies showed that two major phases, i.e., the $SmCo_5$ matrix phase and Sm_2O_3 were present in all the sintered $SmCo_5$ magnets. The presence of Sm_2Co_7 as a minor phase fraction was detected in the sintered $SmCo_5$ magnets containing up to 2 wt.% Ni/Cu. A 2 wt.% Ni/Cu addition to magnets resulted in the presence of two new phases with compositions close to SmCo and Sm_2Co_{17} in addition to $SmCo_5$ and Sm_2O_3 as major phases in the SEM-observed microstructure. These newly formed phases are present in small fractions and are presumably homogenously distributed at the grain boundaries of the magnets. As they are known to act as nucleation sites for reverse magnetic domains, they effectively reduce the intrinsic grain boundary magnetic strength, leading to a drop in the coercivity. We concluded that the sintered $SmCo_5$ magnets could be recycled with up to 2 wt.% Ni/Cu as a residual from the coating under our sintering and heat treatment conditions.

Keywords: $SmCo_5$ magnets; recycling; Ni/Cu coating; magnetic coercivity; microstructure; scanning electron microscopy (SEM)

Citation: Mehmood, M.F.; Eldosouky, A.; Žužek Rožman, K.; Šturm, S. Effects of Ni and Cu Residuals on the Magnetic Properties and Microstructure of $SmCo_5$ Magnets. *Materials* **2022**, *15*, 8226. https://doi.org/10.3390/ma15228226

Academic Editor: Jose Antonio Alonso

Received: 20 October 2022
Accepted: 17 November 2022
Published: 19 November 2022

1. Introduction

Samarium (Sm) and cobalt (Co) are both economic and technically interesting. In addition to their use in permanent magnets, they are found in many other applications such as catalysts, batteries and lasers. Recently, the European Commission identified Sm, among other light-rare-earth elements (LREEs), as being second in terms of supply risk after the heavy rare earth elements. The European Commission will introduce Strategic Foresight Networks to develop robust evidence and scenario planning for raw materials supply, demand and use for strategic sectors in order to integrate the latest knowledge [1]. Recently, Co was also identified as one of the most important elements in terms of green and digital economic value [2,3]. The EU will need up to 5 times more cobalt in 2030, and almost 15 times more cobalt in 2050, to be used in permanent magnets for electric vehicle batteries, energy storage and digital technologies, compared with the current supply to the whole EU economy. If not addressed, this increase in demand will lead to supply issues [4]. Both direct and indirect recycling routes have been emphasized for compounds containing any element of supply risk and with economic importance. At the top are Sm-Co compounds. Indirect recycling consists of the individual separation of elements of interest after leaching. Direct recycling involves the reprocessing of compounds to be used in the same application as the original material.

Samarium–cobalt alloys are a fascinating class of magnetic materials that have an important role in permanent magnetism and modern technology. Since the discovery of high magnetocrystalline anisotropy in the $SmCo_5$ compounds by Strnat and his colleagues in 1966 [5], $SmCo_5$ magnets have been used in many applications, for example, space applications and electronics. Industrially, they usually have an intrinsic coercivity (H_{Ci}) of 1592–2388 kA/m, a maximum energy product (BH_{max}) of 130–245 kJ/m^3 and typical remanence (B_r) values of 0.8–0.96 T [6–8]. The microstructure of $SmCo_5$ magnets consists of $SmCo_5$ as the matrix phase with Sm-rich phases (Sm_2Co_7, Sm_5Co_{19}) and Sm-oxides as randomly distributed phases [9,10]. $SmCo_5$ magnets are considered to be nucleation controlled, and the magnetic coercivity is related to the nucleation of reverse magnetic domains in regions where the anisotropy constant is reduced from the bulk value of the $SmCo_5$ phase. This magnetization reversal takes place at the surfaces of the hard magnetic grains of $SmCo_5$ or at grain boundaries and intergranular phases, which are also regions of reduced magnetocrystalline anisotropy. The lattice imperfections in the $SmCo_5$ matrix might also be preferential sites to begin the magnetic reversal of the grain [11]. It was reported that the interplay between the domain wall pining and nucleation of reverse domains at the grain boundaries and grain boundary phases will affect the coercivity, which depends on a sintering temperature, heat treatment, chemical gradients and impurities [12–16]. A high sintering temperature has the effect of increasing the grain size, which reduces the coercivity, while the postheat treatment of sintered samples at 850–900 °C results in an enhanced coercivity due to the elimination of defects at the atomic level [12]. The presence of traces of the Sm_2Co_{17} phase in the microstructures can serve as sites for the nucleation of reverse domains and therefore decrease the magnet's coercivity [13].

$SmCo_5$ sintered magnets are prepared industrially by milling the as-cast alloy to produce a powder of $\leq$20 µm particle size. This powder is then aligned, pressed and sintered [17,18]. Sintered magnets are usually coated with a mixture of Ni and Cu against corrosion and to improve the mechanical strength during the magnet's handling and final operation. For direct recycling, the magnets should be converted to the powder form; for example, by recasting and milling or hydrogen decrepitation and milling. Although the $SmCo_5Ni_{5-x}$ and $SmCo_5Cu_{5-x}$ systems can have very high H_{Ci} values of up to 20 T measured at room temperatures [19,20], several studies showed that the Ni/Cu-coating residuals have a detrimental effect on the coercivity of a recycled magnet prepared by either of the above processing routes [21].

The goal of this study was to determine the maximum concentration of Ni/Cu-coating residuals present in the recycled $SmCo_5$ powder so that the fabricated, recycled magnets would still have acceptable magnetic properties. Six different mixtures of $SmCo_5$ powders with different Ni/Cu concentrations were prepared and conventionally sintered to produce the magnets. The differences in density, oxygen content, magnetic properties, microstructure and crystal structure of the sintered magnets with different Ni/Cu contents are discussed. The normal coercivity (Hc) is the magnetic field required to reduce the magnetic flux to zero, while the intrinsic coercivity (Hci) is the magnetic field required to reduce the magnetization to zero. It can be measured either empirically or by mathematical analysis. The coercivity of a magnetic material is expressed by the magnetization curve. This can also be called a magnetic hysteresis loop. The hysteresis loop shows how the external magnetizing force and the induced magnetic flux density are related.

For the validity of the comparison, the sintering temperature and heat-treatment profiles were the same for all samples.

2. Materials and Methods

The as-cast Sm-Co alloy with a chemical composition of 36.23 wt. % Sm (18.20 at.% Sm) and 63.77 wt.% Co (81.81 at.% Co) was crushed and milled in a nitrogen atmosphere to produce powder with a particle size of 4–20 µm. Cu and Ni powders (>99.5% purity, Sigma-Aldrich, USA) with a particle size of less than 5 µm were used. First, a mixture of 85 wt.% Ni and 15 wt.% Cu was prepared. This chemical composition of Ni and Cu was

chosen to simulate the coating from the sintered $SmCo_5$ magnet. However, the exact ratio might vary depending on the application procedure and the magnet volume. In the present study, six different mixtures of milled $SmCo_5$ powder with 0, 0.5, 1.0, 2.0, 3.0 and 4.0 wt.% Ni/Cu were prepared. All the mixtures of $SmCo_5$ and Ni/Cu were prepared inside a glove box to prevent the oxidation of the $SmCo_5$ magnet powders. After preparation, the powders were mixed in a tubular mixer for 4 h to ensure complete homogenization. All the prepared mixed $SmCo_5$ + Ni/Cu samples were sintered at 1180 °C for 3 h, cooled down to 880 °C at 1 °C min^{-1} and held for 2 h at this temperature for heat treatment under a partial pressure of 100 mbar of argon (Ar) gas and then cooled to room temperature. The density (ρ) of the samples were measured by Archimedes' principle.

The oxygen (O) content in the samples was measured with an oxygen/nitrogen analyzer (Eltra ON 900, Retsch-Allee, Haan, Germany). For the analysis, 0.2–0.3g of sample were taken in a graphite crucible. The sample was melted in an inert atmosphere of helium (He) gas, carbon from the graphite crucible chemically reacted with the oxygen present in the sample to produce carbon monoxide (CO) gas, which was measured to calculate the oxygen content. The Magnet-Physik's Permagraph (Köln, Germany) with a maximum applied field of 1500 kA/m was used to measure the demagnetization behavior of the previously magnetized samples. An opposite magnetic field was applied to the previously magnetized sample and the polarization of the sample was measured to draw the second quadrant of the hysteresis loop. The instrument required a symmetrical sample with two parallel faces. For the microstructure characterization, a small amount of the magnet powder was mounted in an epoxy mixed with a suitable hardener. The mounted sample was then grinded using a series of silicon carbide grinding sheets having grit sizes of P500, P800, P1000, P2000 and P4000. Then, the sample was polished using cloth sheets and a polycrystalline diamond paste (3 μm and $\frac{1}{4}$ μm). A Struers Tegrapol 15 automatic metallurgical polisher was used for the preparation of the microscope samples for the material's evaluation. During the preparation steps, the samples were continuously checked with a Nikon Eclipse E600POL optical microscope to ensure the grinding efficiency and the removal of scratches. To avoid the charging of the sample by the electron beam, a less-than-10-nm carbon coating was applied using a BAL-TEC SCD 005 Cool Sputter Coater (Switzerland). The carbon coating was applied by evaporation using a heated carbon thread under vacuum. The specimens were then examined for microstructures using a Helios NanoLab™ 650 scanning electron microscope equipped with an energy-dispersive spectrometer (EDS). The elemental distribution was identified with an EPMA-1720 electron probe microanalyzer (EPMA). An operating voltage of 20 kV was used for the microscope.

3. Results and Discussion

3.1. Measurements of Density and Oxygen Content

The density measurement data and oxygen content for all the sintered $SmCo_5$ magnet samples are reported in Table 1. The density values of the sintered $SmCo_5$ with 0–3.0 wt.% Ni/Cu were found to be approximately 8.30 g cm^{-3}, but a value of 8.20 g cm^{-3} was observed for the sample containing 4.0 wt.% Ni/Cu. The theoretical density of a pure $SmCo_5$ magnet is 8.5 gcm^{-3} [20]. The oxygen (O) content in all samples was found to be 0.31–0.325 wt.% O (Table 1). The oxygen content in all the samples was less than 0.35 wt.%, which is acceptable for a $SmCo_5$ magnet [11].

Table 1. Density and oxygen contents of sintered samples of $SmCo_5$ with 0–4 wt% Ni/Cu.

Sintering Conditions	Density (g/cm^3)	Oxygen (wt%)
100 wt% $SmCo_5$	8.30	0.310
99.5 wt% $SmCo_5$ + 0.5 wt% Ni/Cu	8.30	0.325
99.0 wt% $SmCo_5$ + 1.0 wt% Ni/Cu	8.30	0.334
98.0 wt% $SmCo_5$ + 2.0 wt% Ni/Cu	8.30	0.325
97.0 wt% $SmCo_5$ + 3.0 wt% Ni/Cu	8.30	0.314
96.0 wt% $SmCo_5$ + 4.0 wt% Ni/Cu	8.20	0.315

3.2. Magnetic Properties

The demagnetization curves are shown in Figure 1. Because of the magnetometer applied field limitations, we based our mechanism explanations on the demagnetization curve trends, which showed obvious differences in coercivities after simple interpolation. It is true that the full hysteresis loops would provide an even better insight into the demagnetization behavior, but for that, larger demagnetization fields provided via a different magnetometer apparatus would be necessary. Table 2 summarizes the remanence (B_r), energy product (BH_{max}), normal magnetic coercivity (Hc) and intrinsic coercivity (Hc_i) for the sintered $SmCo_5$ magnets. H_c or H_{ci} is called normal coercivity. It is the point on the BH curve where the magnet's internal field is completely cancelled out by the opposing field. In other words, the net flux density is now zero because the opposing field is equal and opposite of the magnet's own field. At this point, the demagnetization is still recoverable because the magnet has not lost its polarity. Up to 2 wt. % Ni/Cu, the magnets showed good magnetic properties with similar demagnetization behaviors. The values of BH_{max} were higher than 150 kJ/m^3 and the H_C values were higher than 640 kA/m. A small increase in the B_r value from 0.92 T to 0.94 T was observed with an increase in the Ni/Cu content up to 2 wt. %, which might be due to a decrease in the Sm_2Co_7 phase content with the Ni/Cu increase, as will be discussed in the next section.

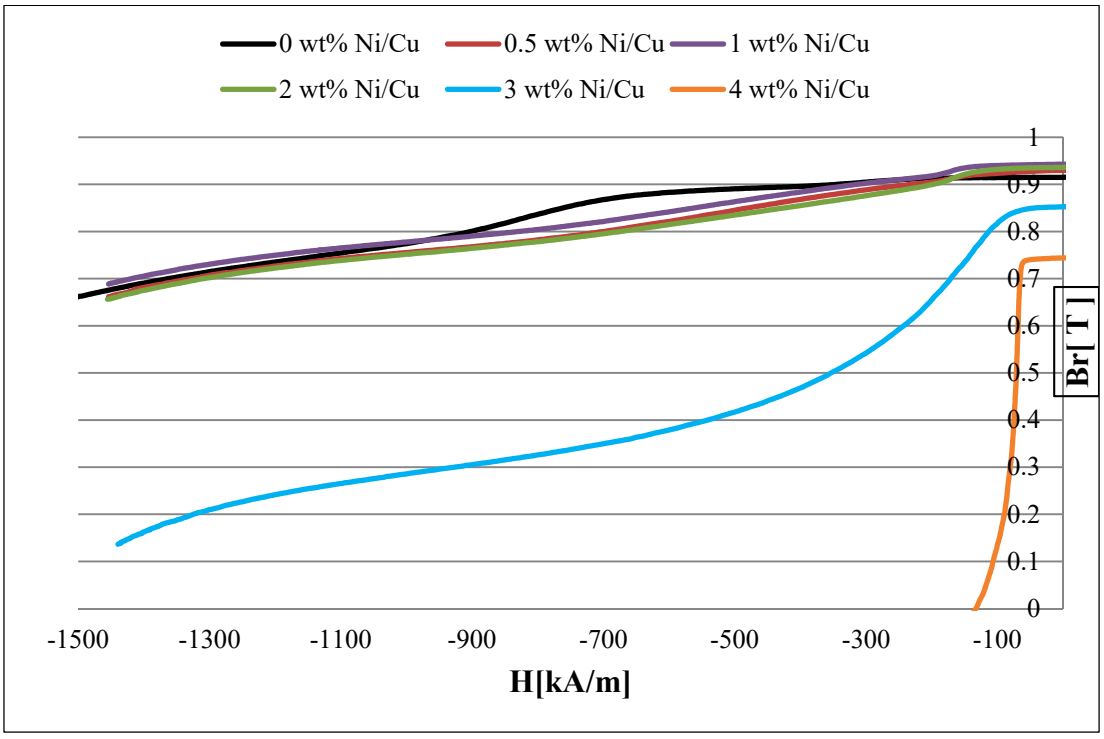

Figure 1. Demagnetization curves for the $SmCo_5$ magnets with 0–4 wt% Ni/Cu contents.

Table 2. Magnetic properties for the magnets with 0–4 wt% Ni/Cu.

Sintering Conditions	BH_{max} [kJ/m^3]	B_r [T]	H_{Ci} [kA/m]	H_C [kA/m]
100 wt% $SmCo_5$	175.1	0.92	>1500	691.8
99.5 wt% $SmCo_5$ + 0.5 wt% Ni/Cu	154.4	0.93	>1500	646.0
99.0 wt% $SmCo_5$ + 1.0 wt% Ni/Cu	159.3	0.94	>1500	660.1
98.0 wt% $SmCo_5$ + 2.0 wt% Ni/Cu	150.3	0.94	>1500	641.7
97.0 wt% $SmCo_5$ + 3.0 wt% Ni/Cu	130.5	0.85	>1500	381.8
96.0 wt% $SmCo_5$ + 4.0 wt% Ni/Cu	23.98	0.74	132.8	101.3

The presence of a large amount of the Sm_2Co_7 phase in the 0 wt. % Ni/Cu might also be the reason for the small shoulder in its demagnetization curve. For the 3 wt. % Ni/Cu magnet, there was a significant decrease in B_r from 0.92–0.94 T to 0.85 T. Moreover, the demagnetization curve had a noticeable shoulder with the decrease in the H_C value to 382 kA/m (Figure 1). This indicates the formation of new phases in the microstructure with a negative effect on the magnetic properties. Consequently, this magnet is unsuitable for applications. Increasing the Ni/Cu concentration further results in the loss of almost all of the magnet's coercivity to a value less than 150 kA/m, with a very low BH_{max} value of 23.98 kJ/m^3 (Table 2).

3.3. Microstructure Characterization

Systematic SEM/EDX analyses of the magnets were performed to correlate the coercivity decrease and the resulting microstructures with different Ni/Cu contents. Figure 2 shows BSE images of the magnets with 0 wt. % to 4 wt.% Ni/Cu. Representative EDX analyses with the corresponding nominal compositions for the phases in the $SmCo_5$ magnets with 0–2 wt.% Ni/Cu and 4 wt.% Ni/Cu contents are shown in Table 3. For the sintered $SmCo_5$ magnets with 2 wt% Ni/Cu, the microstructure is similar (Figure 2a,b) as reported in the literature [9]. The magnets consist of the $SmCo_5$ matrix phase with a random distribution of Sm-rich phases, Sm_2Co_7, Sm oxides and pores that might explain the lower density measured for this sample. The volume ratio of the Sm_2Co_7 phase in the microstructures decreased with increasing Ni/Cu content. The Sm_2Co_7 phase disappeared for the samples with 2, 3 and 4 wt.% Ni/Cu, as observed from the microstructure study (Figure 2d,f). However, this magnet was still showing good magnetic properties, similar to the samples with lower Ni/Cu concentrations. These phases were consistently measured in the sample with 3 wt.% and 4 wt.% of Ni/Cu to be a Sm-rich phase near to the SmCo phase (light gray) and the Co-rich phase with a composition near to Sm_2Co_{17} (dark gray), with partial solubility of the Ni and Cu. The volume fraction of these new phases increased with an increase in the Ni/Cu content. For the 3 wt. % and 4 wt. % Ni/Cu samples, the SmCo and Sm_2Co_{17} phases formed at the grain boundaries and as intergrown clusters. The Sm_2Co_7 phase was not formed in the magnet with 2% Ni/Cu; however, this magnet had good magnetic properties, similar to the samples with a lower Ni/Cu concentration. In some parts of the microstructure of the 2 wt.% Ni/Cu magnet, a new phase of very small fractions (dark grey phase) started to form at the grain boundaries. The distribution of this new phase was shown to increase with an increase in the Ni/Cu. Using the EDX, the composition of the phase was measured in the sample with 4 wt.% Ni/Cu to be a Co-rich phase with a composition close to Sm_2Co_{17}. The fraction of the phase was much higher for the magnet with 4 wt.% Ni/Cu, and this is believed to be the reason for the magnet losing almost all its coercivity. It was concluded that the presence of the impurity phase at the grain boundaries and therefore the decrease in the pinning strength is the main reason for the coercivity drop in the magnets with 4wt.% Ni/Cu in comparison to pristine magnets having the composition of $SmCo_5$, Sm_2CO_7 and the Sm oxide.

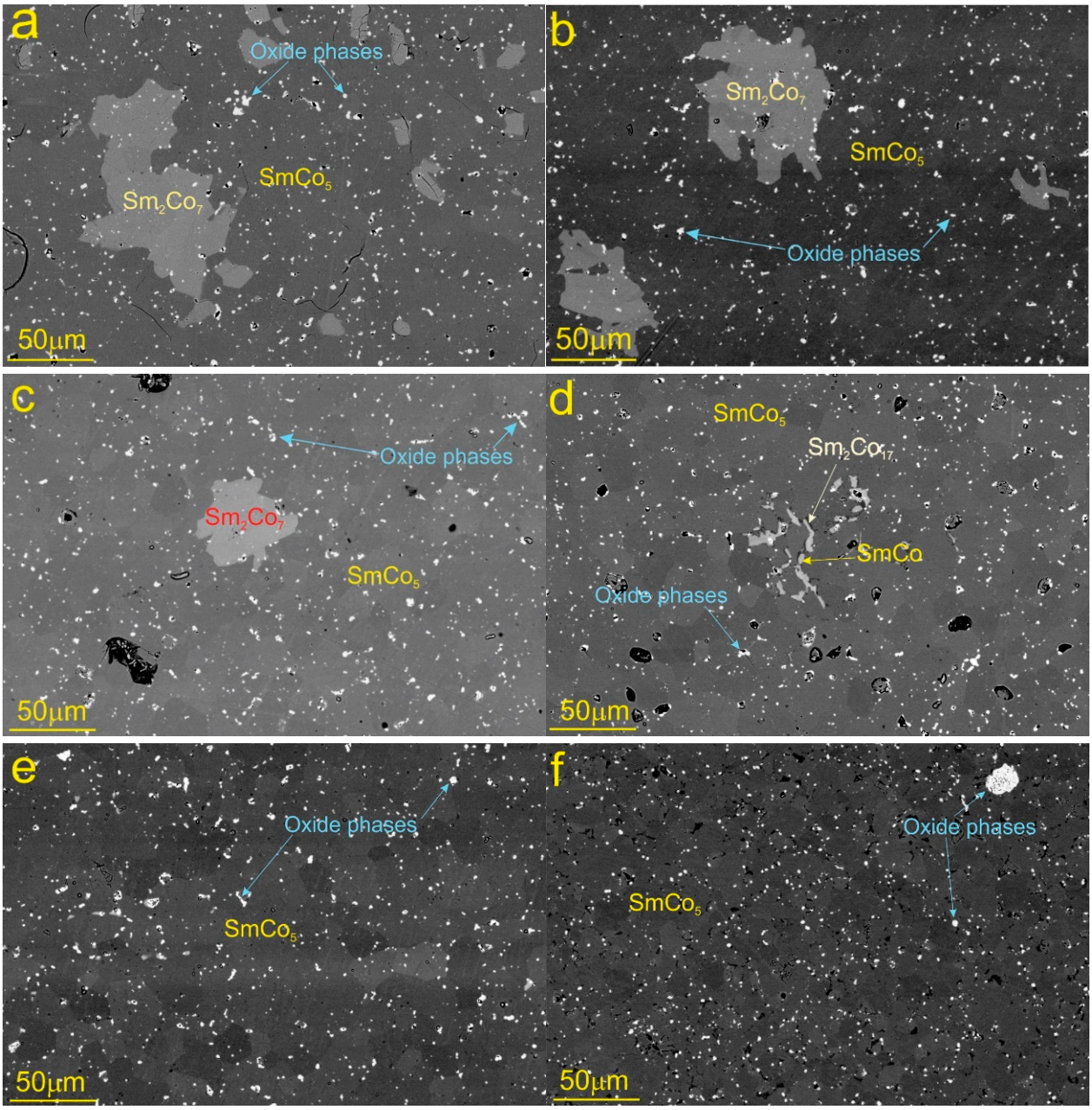

Figure 2. BSE images for the samples with (**a**) 0 wt%, (**b**) 0.5 wt%, (**c**) 1 wt%, (**d**) 2 wt%, (**e**) 3 wt% and (**f**) 4 wt% Ni/Cu, from left to right. For the magnets with Ni/Cu $\geq$ 3 wt%, the SmCo and Sm_2Co_{17} phases were homogeneously distributed in the microstructure, mainly at the grain boundaries, in contrast to the magnet with Ni/Cu of 2 wt% and more where the phases appear only as random clusters.

It is hypothesized that the newly formed phases contribute to a decrease in the pinning strength of the reverse domains in the microstructure, which is translated to the overall coercivity drop. Although some amounts of the SmCo and Sm_2Co_{17} phase can be observed in the magnets with 2 wt.% Ni/Cu fractions, mainly as intergrown clusters, they do not significantly affect the demagnetization behavior of the magnet. This is in striking contrast to the magnets with the highest Ni/Cu contents (4 wt. % Ni/Cu), where these phases could not be observed in the microstructure given the spatial resolution. From these results it is concluded that Ni and Cu do not form any discrete phases with either Sm or Co, as they only replace some of the Co atoms, mainly in the crystal structure of the Sm-Co phases. Xu et al. [22] reported a new design of using the Sm_2Co_7 nanophase to induce

low-temperature hot deformation to prepare $SmCo_5$ magnets. The Sm_2Co_7 nanophase can promote the grain rotation and grain boundary sliding of the $SmCo_5$ phase, thereby coordinating the deformation of the two phases and avoiding local stress concentrations, and finally obtaining a high coercivity magnet with a good c-axis texture under low-temperature hot deformation. Bartlett et al. [23] found that the performance of the $SmCo_5$ magnet deteriorated mainly due to the easier nucleation of the reverse domain due to the precipitation of Sm_2Co_{17}. Chen et al. [18] observed that the 1:5 phase and 2:7 phase coexisted in the spark-plasma-sintered $SmCo_5$ magnet, and a 2:17 phase appeared when the temperature rose to 1050 °C. The best magnetic properties were obtained for the magnets prepared at 1000 °C, with remanence (Br) = 0.45 T, intrinsic coercivity (Hci) = 985 kA/m, and maximum energy density (BH)max = 37 kJ/m^3. The microstructure analysis showed that the high density of the magnet and the uniform distribution of the hard magnetic phase are the main reasons for the excellent magnetic properties. The anisotropy of Sm_2Co_{17} is lower than that of $SmCo_5$ by a factor of about four, but the cellular microstructure of the 2:17 magnets is ideal for coercivity development [24–28].

Table 3. EDX analysis for the phases in the sintered $SmCo_5$ magnet samples with and without Ni/Cu.

Phase	EDX Analysis (at %)					Sm:Co Ratio	Nominal Phase Composition
	Sm	Co	O	Ni	Cu		
Sintered $SmCo_5$ magnet with 0 wt.% Ni/Cu							
Matrix phase	16.8	81.7	1.5	-	-	1:5	$SmCo_5$
Grey phase	22.4	75.9	1.8	-	-	2:7	Sm_2Co_7
White small spots	35.7	11.0	53.3	-	-	*	Sm_2O_3
Sintered $SmCo_5$ magnet with 2 wt.% Ni/Cu							
Matrix Phase	16.2	80.3	0.9	2.3	0.3	1:5	$SmCo_5$
Light Gray Phase	49.3	48.1	1.5	1.3	0.1	1:1	SmCo
Dark Gray Phase	11.2	85.2	0.8	2.4	0.4	2:17	Sm_2Co_{17}
White small spots	30.7	17.0	52.0	0.3	N.D.	*	Sm_2O_3
Sintered $SmCo_5$ magnet with 4 wt.% Ni/Cu							
Matrix Phase	16.0	78.0	1.1	4.2	0.6	1:5	$SmCo_5$
White small spots	36.0	5.0	58.5	0.4	0.1	*	Sm_2O_3

N.D. = Not detectable. * = Sm:O ratio is 2:3 indicating the formation of Sm_2O_3 as small white spots in the microstructure.

Based on the EDX analysis of the elements, the nominal composition of new phases such as $SmCo_{4.75}Ni_{0.25}Cu_{0.04}$, $Sm_2Co_{16.5}Ni_{0.5}Cu_{0.08}$ and $SmCo_{1-x}Ni_x$ can be formulated in the magnet samples containing >2 wt.% Ni/Cu contents by saying the new phases are formed on the account of the Sm_2Co_7 phase. Increasing the Ni/Cu concentration resulted in the change in the $SmCo_5$ and Sm_2Co_7 phase crystal lattice with the partial substitution of Co by Cu and Ni to form new phases. This is known from the literature, as the substitution of Co with Cu in the sintered $SmCo_5$ magnet has already been reported [29–31], and this occurs because of the similar atomic radii of Co (1.52 Å), Ni (1.49 Å) and Cu (1.45 Å) and the same ionic radii of 1.35 Å for Co, Ni and Cu [32,33]. With the increase in the Ni/Cu concentration, the oxygen content increases and forms an Sm-oxide phase, which also results in a decrease in the overall magnetic properties.

4. Conclusions

For sintered $SmCo_5$ magnets to be recycled with no significant reduction in the magnetic properties, the concentration of Ni/Cu-coating residuals should not be more than 2 wt.% for our sintering and heat-treatment conditions. The recycled magnet with a higher Ni/Cu content (4 wt.% Ni/Cu) had a drastic reduction in the magnetic properties, which might be due to newly formed phases, i.e., SmCo and Sm_2Co_{17}, dispersed in the microstructure, contributing to a decrease in the pinning strength of the reverse domains in the microstructure, which is translated to the overall coercivity drop. As they are known to act as nucleation sites for the reverse domains, they effectively decrease the intrinsic

grain-boundary magnetic strength, controlling the overall coercivity. We conclude that the recycling of permanent magnets for the sustainable production of permanent magnets with a sintering route is possible.

Author Contributions: Conceptualization, M.F.M.; methodology, M.F.M.; software, M.F.M.; validation, M.F.M. and S.Š.; formal analysis, M.F.M.; investigation, M.F.M.; resources, M.F.M., A.E. and S.Š.; data curation, M.F.M.; writing—original draft preparation, M.F.M.; writing—review and editing, M.F.M., A.E., S.Š. and K.Ž.R.; visualization, M.F.M.; supervision, S.Š. and K.Ž.R.; project administration, S.Š. and K.Ž.R.; funding acquisition, S.Š. and K.Ž.R. All authors have read and agreed to the published version of the manuscript.

Funding: The study leading to these results received funding from the European Community's Horizon 2020 Programme (H2020/2014–2019) under Grant Agreement No. 674973 (MSCA-ETN DEMETER). Project website: http://etn-demeter.eu/ (accessed on 19 October 2022), and of Slovenian Research agency via P2-0084 and L2-9213. This publication reflects only the authors' research findings, which are targeted to contribute to the betterment of the global community.

Acknowledgments: The authors duly acknowledge the Center for Electron Microscopy and Microanalysis (CEMM) for supporting the scanning electron microscopy analysis at the Jožef Stefan Institute, Slovenia.

Conflicts of Interest: The authors declare that this research was performed in the absence of any commercial or financial relationships that could be interpreted as a potential conflict of interest.

References

1. European Commission. *Communication from the Commission to the European Parliament, The Council, The European Economic and Social Committee and the Committee of the Regions: Critical Raw Materials Resilience: Charting a Path towards Greater Security and Sustainability*; COM (2020) 474 final; European Comission: Brussels, Belgium, 2020; pp. 1–23.
2. European Commission. *Report on Critical Raw Materials for the EU, Report of the Ad Hoc Working Group on Defining Critical Raw Materials*; European Comission: Brussels, Belgium, 2014; pp. 1–41.
3. Gislev, M.; Grohol, M. *European Commission. Report on Critical Raw Materials in the Circular Economy*; Publications Office: Brussels, Belgium, 2018; pp. 1–80. [CrossRef]
4. Dias, P.A.; Blagoeva, D.; Pavel, C.; Arvanitidis, N. *Cobalt: Demand-Supply Balances in the Transition to Electric Mobility. JRC Science for Policy Report*; European Commission: Brussels, Belgium, 2018. [CrossRef]
5. Strnat, K.; Hoffer, G.; Olson, J.; Ostertag, W.; Becker, J.J. A family of new cobalt base permanent magnet materials. *J. Appl. Phys.* **1967**, *38*, 1001–1002. [CrossRef]
6. Pan, S. *Rare Earth Permanent-Magnet Alloys' High Temperature Phase Transformation: In Situ and Dynamic Observation and Its Application in Material Design*; Springer: Heidelberg, Germany; Dordrecht, The Netherlands; London, UK; New York, NY, USA, 2013; ISBN 978-3-642-36387-0.
7. Kumar, K.; Das, D.; Wettstein, E. High coercivity, isotropic plasma sprayed samarium-cobalt magnets, J. *Appl. Phys.* **1978**, *49*, 2052–2054. [CrossRef]
8. Coey, J.M.D. *Magnetism and Magnetic Materials*; Cambridge University Press: Cambridge, UK, 2010. [CrossRef]
9. Szmaja, W.; Polanski, K.; Piwonski, I.; Ilik, A.; Balcerski, J. Study of the morphological and magnetic microstructure of $SmCo_5$ magnets. *Vacuum* **2007**, *81*, 1363–1366. [CrossRef]
10. Riley, A. The microstructure of $SmCo_5$ sintered magnet material. *J. Less Common Met.* **1976**, *44*, 307–317. [CrossRef]
11. De Campos, M.F.; Landgraf, F.J.G.; Saito, N.H.; Romero, S.A.; Neiva, A.C.; Missell, F.P.; de Morais, E.; Gama, S.; Obrucheva, E.V.; Jalnin, B.V. Chemical composition and coercivity of $SmCo_5$ magnets. *J. Appl. Phys.* **1998**, *84*, 368–373. [CrossRef]
12. Das, D.K. Influence of sintering temperature on magnetic properties of samarium-cobalt magnets. *IEEE Trans. Magn.* **1971**, *7*, 432–435. [CrossRef]
13. De Campos, M.F.; Okumura, H.; Hadjipanayis, G.C.; Rodrigues, D.; Landgraf, F.J.G.; Neiva, A.C.; Romero, S.A.; Missell, F.P. Effect of several heat treatments on the microstructure and coercivity of $SmCo_5$ magnets. *J. Alloys Compd.* **2004**, *368*, 304–307. [CrossRef]
14. Kumar, K. $RETM_5$ and RE_2TM_{17} permanent magnets development. *J. Appl. Phys.* **1988**, *63*, R13–R57. [CrossRef]
15. Zhang, D.-T.; Zhu, R.-C.; Yue, M.; Liu, W.-Q. Microstructure and magnetic properties of $SmCo_5$ sintered magnets. *Rare Met.* **2019**, *39*, 1295–1299. [CrossRef]
16. De Campos, M.F.; Landgraf, F.J.G.; Machado, R.; Rodrigues, D.; Romero, S.A.; Missell, F.P. A modeling relating remanance and microsctructure of $SmCo_5$ magnets. *J. Alloys Comp.* **1998**, *267*, 257–264. [CrossRef]
17. Nie, J.; Han, X.; Du, J.; Xia, W.; Zhang, J.; Guo, Z.; Yan, A.; Li, W.; Liu, J.P. Structure and magnetism of $SmCo_5$ nanoflakes prepared by surfactant-assisted ball milling with different ball sizes. *J. Magn. Magn. Mater.* **2013**, *347*, 116–123. [CrossRef]
18. Chen, Y.; Jiang, Q.; Li, X.; Rehman, S.U.; Zhao, C.; Song, J.; Zhong, Z. Influence of sintering temperatures on the phase structure and magnetic properties of spark plasma sintered $SmCo_5$ magnets. *J. Supercond. Nov. Magn.* **2021**, *34*, 3395–3401. [CrossRef]

19. Prados, C.; Hadjipanayis, G.C. Magnetic and structural properties of high coercivity Sm(Co, Ni, Cu) sputtered thin films. *J. Appl. Phys.* **1998**, *83*, 6253. [CrossRef]
20. Oesterreicher, H.; Parker, F.T.; Misroch, M. Temperature and time dependence of giant intrinsic magnetic hardness in $SmCo_{5-x}Ni_x$. *Physica B+C* **1977**, *86–88*, 1475–1476. [CrossRef]
21. Eldosouky, A.; Škulj, I. Recycling of $SmCo_5$ magnets by HD process. *J. Magn. Magn. Mater.* **2018**, *454*, 249–253. [CrossRef]
22. Xu, X.C.; Li, Y.Q.; Ma, Z.H.; Yue, M.; Zhang, D.T. Sm_2Co_7 nano-phase inducing low-temperature hot deformation to fabricate high performance $SmCo_5$ magnet. *J. Scr. Mater.* **2020**, *178*, 34–38. [CrossRef]
23. Bartlett, R.W.; Jorgensen, P.J. Microstructural changes in SmCo5 caused by oxygen, sinter-annealing and thermal aging. *J. Less Common Met.* **1974**, *37*, 21–34. [CrossRef]
24. Duerrschnabel, A.M.; Yi, M.; Uestuener, K.; Liesegang, M.; Katter, M.; Kleebe, H.-J.; Xu, B.; Gutfleisch, O.; Molina-Luna, L. Atomic structure and domain wall pinning in samarium-cobalt-based permanent magnets. *Nat. Commun.* **2017**, *8*, 54. [CrossRef]
25. Skomski, R. Domain-wall curvature, and coercivity in pinning-type Sm-Co magnets. *J. Appl. Phys.* **1997**, *81*, 5627. [CrossRef]
26. Katter, M. Coercivity calculation of $Sm_2(Co,Fe,Cu,Zr)_{17}$ magnets. *J. Appl. Phys.* **1998**, *83*, 6721. [CrossRef]
27. Streibl, B.; Fidler, J.; Schrefl, T. Domain wall pinning in high-temperature $Sm(Co,Fe,Cu,Zr)_{7-8}$ magnets. *J. Appl. Phys.* **2000**, *87*, 4765. [CrossRef]
28. Scholz, W.; Fidler, J.; Schrefl, T.; Suess, D.; Matthias, T. Micromagnetic three-dimensional simulation of the pinning field in high-temperature Sm(Co,Fe,Cu,Zr)z magnets. *J. Appl. Phys.* **2002**, *91*, 8492. [CrossRef]
29. Haider, S.K.; Ngo, H.M.; Kim, D.; Kang, Y.S. Enhancement of anisotropy energy of $SmCo_5$ by ceasing the coupling at 2c sites in the crystal lattice with Cu substitution. *Sci. Rep.* **2021**, *11*, 10063. [CrossRef] [PubMed]
30. Lamichanne, M.; Rai, B.K.; Mishra, S.R.; Nguyen, V.V.; Liu, J.P. Magnetic properties hard-soft $SmCo_5$-FeNi and $SmCo_5$-FeCo composites prepared by electroless coating technique. *Open J. Compos. Mater.* **2012**, *2*, 119–124. [CrossRef]
31. Hadjipanayis, G.C.; Prados, C.; Hernando, A. Nanocrystalline Sm-Co-Cu(Ni) thin films with giant coercivity. *Nanostructured Mater.* **1999**, *12*, 1161–1166. [CrossRef]
32. Clementi, E.; Raimondi, D.L. Atomic screening constants from SCF functions. *J. Chem. Phys.* **1963**, *38*, 2686–2689. [CrossRef]
33. Shannon, R.D.; Prewitt, C.T. Effective ionic radii on oxides and fluorides. *Acta Crystallogr. Sect. B Struct. Sci. Cryst. Eng. Mater.* **1969**, *25*, 925–946. [CrossRef]